

Optimization and effect of UV-ozone exposure of electron transport layer on the efficiency of the dye-sensitized solar cells

Chandan Dawo^a, Mohammad Adil Afroz^b, Parameswar Krishnan Iyer^{b,c} and Harsh Chaturvedi^{*a}

^aCentre for Energy, Indian Institute of Technology Guwahati, Guwahati 781039, Assam, India

^bDepartment of Chemistry, Indian Institute of Technology Guwahati, Guwahati 781039, Assam, India

^cCentre for Nanotechnology, Indian Institute of Technology Guwahati, Guwahati 781039, Assam, India

Corresponding Author: *Harsh Chaturvedi, email: harshc@iitg.ac.in

KEYWORDS: Electron transport layer, ultraviolet-ozone, dye sensitized solar cell, organic contaminants, hydrophilicity.

ABSTRACT:

The surface states of the active TiO₂ layer is crucial while fabricating an efficient solar cell. This work experimentally analyses the effect of exposing TiO₂ based electron transport layer (ETL) to the ultraviolet-ozone (UV-O₃) and optimizes the exposure time for improving power conversion efficiency (PCE) of fabricated dye-sensitized solar cells (DSSCs). These results demonstrate that the performance of DSSCs can be improved significantly by UV-O₃ exposure of sintered TiO₂ photoanode surface, with the duration of exposure being a critical parameter. Fabricated devices show 33.01 % increase in PCE for the optimum exposure. Nevertheless, overexposure of the sample beyond the optimum time decreases the efficiency of the fabricated solar cells. The device with optimum exposure exhibits the highest PCE of 8.34% with short circuit current density (*J*_{sc}) of 15.15 mA/cm², open circuit voltage (*V*_{oc}) of 756 mV and Fill factor (FF) of 71.10%. This increase in efficiency is attributed to the enhanced crystallization and reduction in the organic contaminants C-C/C-H from 57.90 to 52.40% as shown by the X-ray diffraction (XRD) and X-ray

photoelectron spectroscopy (XPS), respectively. The XPS result further indicates an increase in oxygen vacancy from 12.40 to 23.40% for O 1s state and from 9.30 to 14.30% for Ti 2p state of Ti^{3+} . Results from the Atomic Force Microscope (AFM) also confirms the minimized surface roughness of 16.36 nm for the optimally exposed TiO_2 film, and increase in hydrophilicity leading to improved efficiency of the solar cells which were optimally exposed to UV- O_3 .

1. INTRODUCTION

Grätzel and O'Reagan developed dye-sensitized solar cells (DSSCs) in 1991 with mesoporous TiO_2 film as photoanode [1]. Since then, DSSCs have drawn the attention of the scientific community because of its low materials cost, easy fabrication process, lightweight, flexibility, tunable optical properties, and raw materials availability. DSSCs are generally composed of mesoporous TiO_2 photoanode to uptake dye photosensitizer, liquid electrolytes (I^-/I_3^-), and platinum (Pt) counter electrode. So far, $\approx 13\%$ efficiency has been reported for DSSCs based on TiO_2 photoanode [2,3].

The most preferred photoanode material for DSSC is nanocrystalline TiO_2 due to its electro-optical characteristics i.e., favourable valence band and conduction band position for dye and FTO, chemical stability, high refractive index (2.45), cost-effectiveness, strong oxidizing power, mesoporous nature and low toxicity [4-6]. TiO_2 based photoanode plays multiple roles for efficient charge generation, charge separation, and charge transfer from dye molecule to transparent conducting oxide (TCO) substrate. The conversion of light to electricity consists of multiple dynamic processes in DSSCs. Several undesired recombination processes are also known to occur at the photoanode, significantly reducing the PCE. Minimizing such unwanted processes at the active layer of TiO_2 is required for the efficient performance of the DSSCs. Hence, the surface states of the active layer of TiO_2 plays an important role in the fabrication of an efficient solar cell [7-11].

Several modifications of the TiO_2 photoanode have been reported to increase the efficiency of DSSCs, such as compact or blocking layer [12-14], scattering layer [15], atomic doping [16, 17], surface treatment [18], etc. The surface treatment of TiO_2 electron transport layer (ETL) has become an essential step for improving the performance of DSSCs. Surface treatment of the photoanode affects dye loading capacity, electron transport, and electron recombination processes. $TiCl_4$ treatment on the TiO_2 ETL has been the most commonly applied method to increase

efficiency of DSSCs [19-21]. However, TiCl_4 is not stable at room temperature as it reacts with moisture present in the air to produce the harmful hydrochloric acid [22]. A simple post-treatment of TiO_2 photoanode by urea solution with a concentration of 1 g/mol showed improvement in the efficiency of solar cells [23]. A comparative study of oxygen plasma treatment and oxygen ion beam treatment has reported that Oxygen ion beam treatment of DSSCs shows higher efficiency than plasma treatment. As it is much more efficient in removing the number of oxygen vacancies from a TiO_2 active film [24]. Deposition of various other layers of $\text{Ba}(\text{NO}_3)_2$, $\text{N}_2\text{O}_6\text{Sr}$, and $\text{Mg}(\text{NO}_3)_2$, on TiO_2 electrode followed by an O_2 plasma treatment, also shows significant improvement in the photo-conversion efficiency of the DSSCs [25]. Oxygen (O_2) plasma treatment of TiO_2 ETL, remarkably increase in the performance of DSSCs [26]. The drawback of oxygen plasma treatment, however, is its cost, which requires considerable capital investment. Therefore, UV- O_3 treatment provides an effective and economical alternative method [27].

In this study, an attempt has been made to study and optimize the effect of UV- O_3 exposure on a uniform TiO_2 ETL leading to DSSCs with higher efficiency. The samples were exposed to UV- O_3 for different duration of times (0, 5, 10, 15, and 30 min), under ambient conditions, and keeping other parameters constant. The results demonstrate that by optimizing the exposure time, we can effectively control the stoichiometry of these samples. This results in an optimized condition affecting optical absorption, wettability, crystallinity, surface morphology, electrical conductivity etc., thereby improving the overall carrier dynamics of the prepared TiO_2 film. Consequently, at the optimum condition of 10 min exposure, the PCE of DSSCs shows significant improvement to 8.34% as compared to the untreated device with a PCE of 6.27 %.

2. EXPERIMENTAL

2.1 Chemicals and Materials

All chemicals and reagents purchased for the experiments were used as received and obtained from different commercial sources: FTO (Fluorine doped tin oxide) glass- 7 Ω /square sheet resistance (Sigma- Aldrich), TiO_2 nanoparticles (Degussa P25, Sigma-Aldrich, 21 nm), TiO_2 Paste (Sigma-Aldrich, 22 nm), terpeneol (Sigma- Aldrich), tert-butanol (Sigma- Aldrich), acetonitrile (fisher scientific), absolute ethanol (Changshu yangyuan chemical, China) , acetic acid (Merck), ethyl cellulose (Himedia), iodine (Himedia), lithium iodide (Sigma-Aldrich), valeronitrile (sigma-

Aldrich), 4-tert butylpyridine (Sigma-Aldrich), 1-butyl-3-methylimidazolium iodide (Sigma-Aldrich), NaOH (Merck), Chloroplatinic acid hexahydrate ($\text{H}_2\text{PtCl}_6 \cdot 6\text{H}_2\text{O}$, Sigma-Aldrich), Anhydrous isopropanol (Sigma-Aldrich).

2.2 Preparation of TiO_2 Working Electrode

FTO substrates were cleaned using 15 min ultrasonication in Mili-Q water, acetone, and 2-propanol, respectively. Cleaned and hot air dried FTO coated substrate was then exposed to UV- O_3 treatment for 15 min to remove any organic contaminants. The mesoporous layer of TiO_2 consists of two layers. The TiO_2 paste consists of 600 mg P25 powder, 5 mL ethanol, 100 μL acetic acid, 500 μL milli-Q water, 3 gm tarpineol, and 3 gm ethyl cellulose (15 wt. % in ethanol). The mixture was stirred overnight and spin-coated at 5000 rpm for 45 secs on the clean substrate. After drying the first layer of TiO_2 at 100 °C for 10 min, the second layer of TiO_2 was applied by the doctor blade technique using Sigma paste and baked at 100 °C for 20 min. Samples were then sintered at 500 °C for 30 min to improve the interfacial contact between the deposited TiO_2 layer and the FTO substrate. TiO_2 , which acts as a layer for electronic transport, was exposed to UV- O_3 for different time durations (0, 5, 10, 20, and 30 min). A set of 10 samples were prepared for each time interval to confirm the reproducibility of the experiment.

2.3 Fabrication of the Dye-sensitized solar cell

The working TiO_2 photoanodes with and without UV- O_3 treatment were dipped into N719 dye solution (0.3 mM N719 in tert-butyl alcohol and acetonitrile, volume ratio 1:1) and kept for 24 hours to sensitize it at ambient condition. The Pt counter electrode was fabricated on another pre-cleaned FTO substrate by spin coating chloroplatinic acid hexahydrate solution (5 mg $\text{H}_2\text{PtCl}_6 \cdot 6\text{H}_2\text{O}$ in 1 ml of anhydrous 2-propanol) at 5000 rpm for 45 secs followed by annealing at 500 °C for 30 min. The solution of I^-/I_3^- electrolyte was made with 0.5M LiI, 0.05M I_2 , 0.5M 1-Butyl-3-methylimidazolium iodide, 0.1M guanidium thiocyanate, and 0.5M 4-tert-butylpyridine dissolved in the mixture of acetonitrile/valeronitrile (v/v= 85:15) solvent. DSSCs were assembled between dyed TiO_2 photoanode and Pt counter electrode using a hot melt spacer (Surlyn film, 60 μm , purchased from ossila). The interspace available between the TiO_2 photoanode and the counter electrode was then filled with a liquid electrolyte to complete the fabrication of DSSCs. The active area of DSSCs was 0.09 cm^2 .

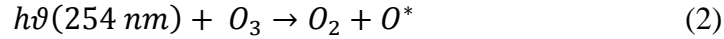
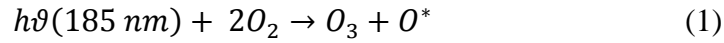
2.4 Characterization

X-ray photoelectron spectroscopy (XPS) was used to study the structural and chemical changes of TiO₂ film, exposed to the UV-O₃ system for a different duration. The absorption spectra of thin-film TiO₂ photoelectrodes sensitized with N719 dye was measured with diffused reflectance UV-vis spectrometer (Lambda 950). The TiO₂ films with dimensions of 0.5 cm x 1.0 cm and a thickness of 8.5 μm were soaked in 3 mL of 0.1 M NaOH solution in ethanol and DI water (volume ratio of 1:1) to desorb the dye from the film and absorption spectra was taken by means of UV-vis spectrometer (Cary 100). With the help of an automatic liquid dispenser at room temperature, contact angle measurements were done by KRÜSS Drop Shape Analyser (DSA25). The root mean square (RMS) roughness was computed with atomic force microscopy (Agilent 5500-STM). The phase and crystal structure of the TiO₂ ETL films was analysed by X-ray diffraction (XRD) with an operating voltage of 45 KV and 200 mA current using Rigaku SmartLab with Cu-K α radiation ($\lambda=1.54\text{\AA}$). The TiO₂ thin films were scanned from 20° to 70° of 2 θ with a scan rate of 5 degrees/min. The electrical characteristics of DSSCs were measured with a Keithley 2400 source meter from -1 to 1V in a step of 10 mV, under AM 1.5 G (100 mW/cm²) illumination, which was provided by a solar light simulator (Newport, Oriel Sol 3A). The light intensity of the solar simulator was calibrated with a standard silicon solar cell of the National Renewable energy laboratory (NREL). Using an electrochemical workstation (CH 680), the electrochemical impedance spectra (EIS) of DSSCs were measured in a bias potential particularly at open circuit voltage under dark conditions, in the frequency ranges of 0.1 Hz to 1 MHz with a small alternating signal of amplitude 10 mV. The impedance parameters of the equivalent circuit were determined by fitting the spectra using EC Lab software.

2.5 UV-O₃ exposure on TiO₂ ETL

UV-O₃ exposure was performed using NOVASCAN PSD Pro UV system. The UV-O₃ system produces ultraviolet light of two wavelengths, 254 and 185 nm simultaneously with very high photon energy of 470 and 647 kJ/mol, respectively. The bond energy of the organic contaminants C-C, C-H, C-O and O-H are 346, 411, 358 and 459 kJ/mol, respectively. The photon energies irradiated from the UV-O₃ system are much higher than the bond energies of contaminants. Therefore, the organic contaminant molecules are dissociated or excited by the irradiation of UV light. The atmospheric oxygen (O₂) is irradiated with ultraviolet rays at 185 nm; after absorption,

it converts to atomic oxygen (O^*) and ozone (O_3) (equation 1), whereas O_3 decomposes after irradiation with 254 nm UV light (equation 2). Strong oxidizing atomic oxygen (O^*) is generated during the process of decomposition or formation of O_3 . Atomic oxygen and O_3 strongly react with organic materials to produce volatile molecules such as CO_2 , H_2O , N_2 etc. The samples treatment was performed at normal atmospheric pressure and room temperature [28, 29].



3. RESULTS AND DISCUSSION

The structural and chemical changes on the TiO_2 ETL were studied by XPS upon UV- O_3 exposure. Fig. 1a, b demonstrates the XPS spectra of carbon contaminants present in TiO_2 film for 0- and 10-min UV- O_3 treatment. The C 1s peak intensity found at 284.8 eV decreased significantly after UV- O_3 exposure. This suggests that UV- O_3 treatment burns out organic contaminants from the precursor of TiO_2 film [30, 31]. The quantitative analysis of carbon atom percent, C-C/C-H peak area decreased from 57.90% to 52.40% after UV- O_3 treatment (Table S1). The relative changes in the peak area reveals that chemical environment of TiO_2 film changes with UV- O_3 exposure. Carbon contamination acts as interfacial trap sites and decreases cell performance. It affects the anchoring of dye molecules on TiO_2 film, which results in less quantity of dye adsorbed and therefore produces less photocurrent, fill factor, and efficiency. The O 1s peak of TiO_2 film without and with UV- O_3 treatment was fitted with two Gaussian peaks (Fig. 1c, d). The central O 1s peak found at 529.99 eV corresponds to the lattice oxygen of TiO_2 (Ti^{4+}). The higher binding energy on shoulder peak at 531.3 eV \pm 0.2 eV is attributed to the formation of Ti^{3+} surface state through the creation of oxygen vacancies, commonly written as Ti_2O_3 . The change of oxidation state from Ti^{4+} to Ti^{3+} occurred due to O^- and O_2^- species introduced on the surface of TiO_2 by UV- O_3 exposure [32-35]. The ratio of the atom percent calculated from the Ti_2O_3 peak area increases from 12.40% (0 min) to 23.4% (10 min) after the UV- O_3 treatment (Table S1). Oxygen vacancies generated from the reduction of Ti^{4+} to Ti^{3+} produces electrons, thereby affecting the surface functionality and charge state of the TiO_2 ETL. The excess number of electrons generated by UV- O_3 treatment helps in efficient charge transport and substantial reduction in electron-hole recombination rate as inferred through impedance measurements. Fig. 1e, f illustrates the XPS spectra of Ti 2p for TiO_2 samples. For 0 and 10 min UV- O_3 exposure, the TiO_2 sample shows peaks at 457.5 \pm 0.1 eV, and

463±0.2 eV corresponding to the binding energy level of $Ti^{4+} 2p_{3/2}$ and $Ti^{4+} 2p_{1/2}$, along with the peaks at 456.4 eV ±0.1 eV and 458.5 eV ± 0.2 eV imputed to $Ti^{3+} 2p_{3/2}$ and $Ti^{3+} 2p_{1/2}$ energy level of Ti^{3+} state respectively [18, 31, 36, 37].

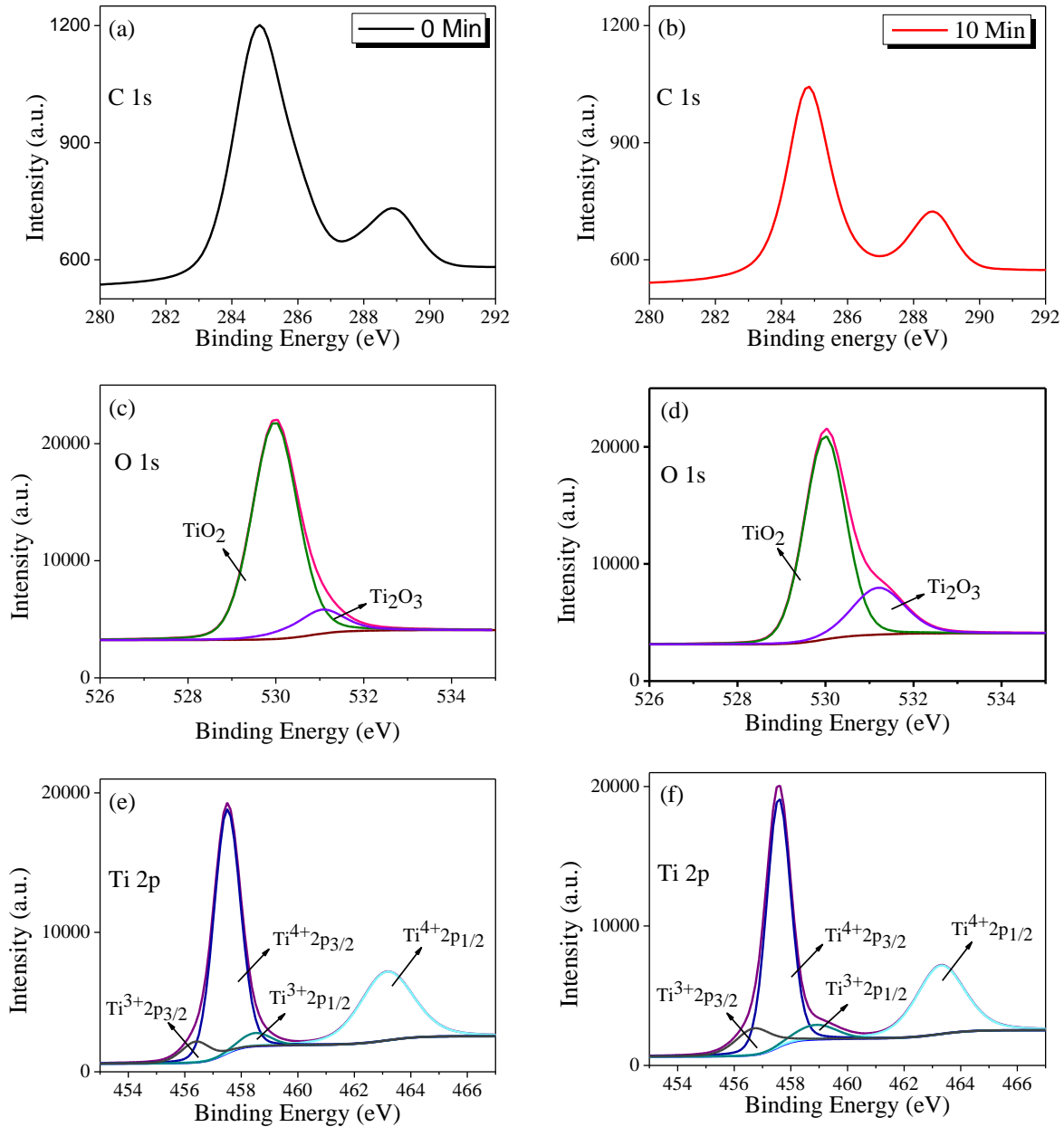


Fig. 1: XPS spectra of TiO₂ films on FTO glass substrates : (a, c, and e) with 0 min, and (b, d, and f) with 10 min UV-O₃ treatment.

Peak areas of $Ti^{3+}2p_{3/2}$ state increases by 59.60% and $Ti^{3+}2p_{1/2}$ by 44.44% respectively after UV- O_3 treatment (Table S1). The difference in these peak areas is attributed to the change in the stoichiometry of the TiO_2 film; due to increase in the number of oxygen vacancies by UV- O_3 exposure.

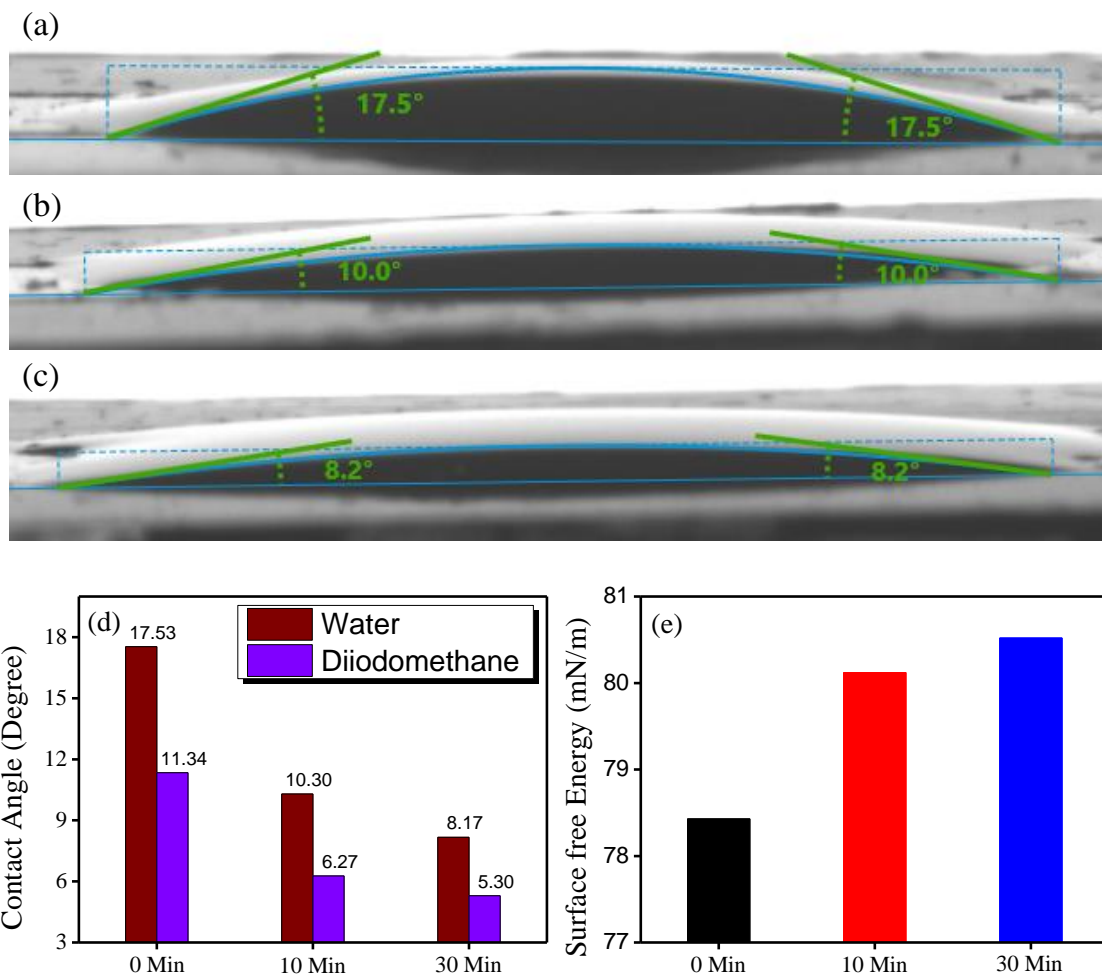


Fig. 2. Contact angle analysis pattern of water on TiO_2 films with (a) 0 min (b) 10 min and (c) 30 min UV- O_3 exposure. Variation of (d) contact angle and (e) Surface free energy by UV- O_3 treatment time.

The contact angle of TiO_2 active layer films were measured using KRÜSS Drop Shape Analyser instrument at ambient conditions. Deionized (DI) water (H_2O) and Diiodo-methane (CH_2I_2) were used as the test liquids. The test liquid was placed at different locations on TiO_2 active surface. Once the drop achieved metastable equilibrium, the measurement was carried out. Three measurements were taken from each sample, and the mean contact angle value is used to

calculate the Surface free energy (SFE). The dispersive and polar components of the surface free energy were computed from the measured contact angles of DI water and Diiodo-methane using KRÜSS advance software (Table S2). The following equation was used to calculate the total SFE (equation 3) [38].

$$\gamma_s = \gamma_s^d + \gamma_s^p \quad (3)$$

Where γ_s is the SFE, γ_s^d , and γ_s^p are the dispersive and polar component of the SFE of the examined TiO₂ films.

Fig. 2a, b, c demonstrates the contact angle analysis of TiO₂ photoanodes after sintering without and with UV-O₃ irradiation. The contact angle reduces from $17.5 \pm 0.5^\circ$ to $8.2 \pm 1^\circ$ after 30 min of UV-O₃ exposure as shown in Fig. 2d. Decrease in the contact angle (Fig. 2a, b, c) indicates increase in hydrophilicity and corresponding increase in surface free energy (Fig. 2e). This increase in surface energy is attributed to the removal of unwanted hydrophobic organic components and the increase of hydrophilic oxygen vacancies in TiO₂ film [34, 39-41].

Atomic force microscopy (AFM) was utilized to analyse the surface topography and roughness/sectional profile of TiO₂ ETL film exposed to UV-O₃ system for different durations (Fig. 3a, b, c.). The root mean square (RMS) roughness decreases by 27.22 % for 10 min exposure as compared to unexposed sample. However, roughness further increases by 19.52 % for 30 min exposure. High roughness factor and irregular pores affect crystallization properties, increase the

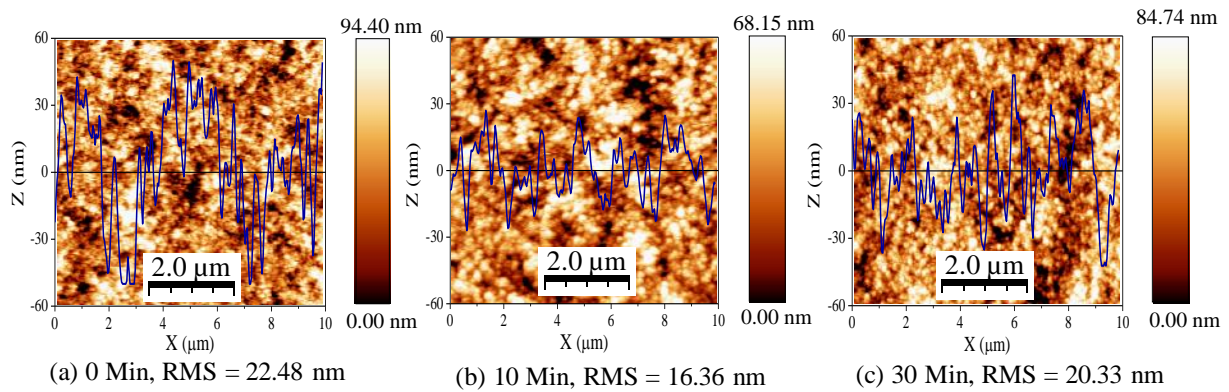


Fig. 3: Two-dimensional AFM images and sectional profile of TiO₂ film with (a) 0 min, (b) 10 min, and (c) 30 min UV-O₃ exposure.

grain size of the TiO₂ film [39, 42]. 10 min UV-O₃ exposure has the lowest surface roughness indicating smooth, uniform pores and compact surface films, leading to efficient harvesting of light, better accessibility of dye adsorption, and prevents direct contact between TiO₂ and dye molecules thereby resulting in high conversion efficiency. The highest conversion efficiency in perovskite solar cells was also achieved for the sample with lowest RMS value [33].

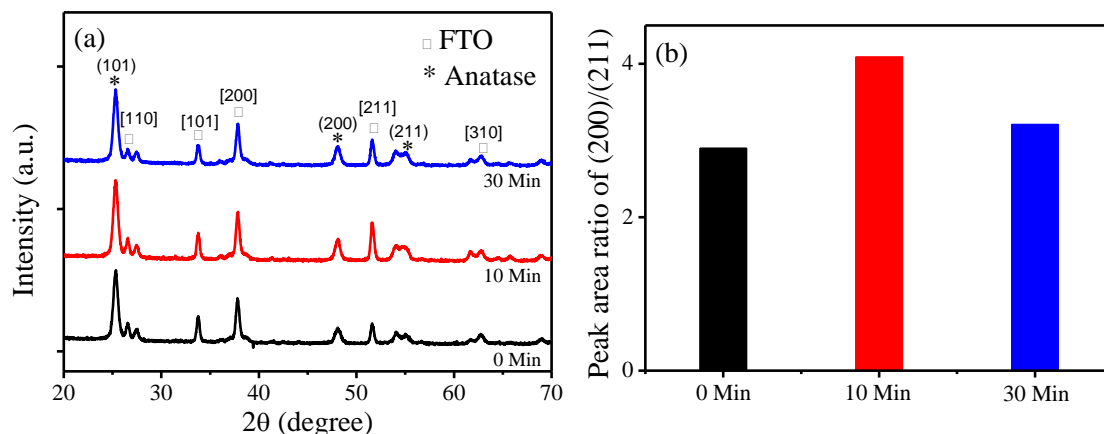


Fig. 4: X-ray diffraction spectra of TiO₂ film with (a) 0, 10, and 30 min UV-O₃ exposure. (b) Peak area ratio of (200)/ (211) plane.

Fig. 4a displays the XRD pattern of TiO₂ film with different UV-O₃ treatment time. All samples show diffraction peaks of (101), (200), and (211) planes at corresponding Bragg angles of 25.35°, 48.06°, and 55.00° respectively, and are of anatase phase [8, 43]. The diffraction pattern of TiO₂ ETL photoanode with different UV-O₃ treatment times remains almost the same, with slight difference in intensity and relative peak area. The highest intensity and relative peak area are observed for 10 min UV-O₃ treatment. Changes in the relative peak area are presented in Table S3. Relative area of (211) plane decreased from 10.16% to 6.20% after UV-O₃ treatment for 10 min. The highest ratio of 4.09 for (200)/ (211) plane peak area is shown in Fig. 4b. From the relative peak area analysis, it can be concluded that UV-O₃ treatment affects the orientation of mesoporous TiO₂ ETLs. Favourable atomic arrangement of (101) and (200) orientation leads to improve crystallinity and better interconnection between the TiO₂ nanoparticle and FTO.

The changes in the photocatalytic activity were examined using the UV-visible spectrometer. Fig. 5a shows the diffused reflectance UV-Vis absorption spectra of N719 sensitizer anchored on TiO₂ photoanode. The photoanode absorption spectra shows two metal-to-ligand charge-transfer (MLCT) peak at 534 nm and 400 nm. Fig. 5b illustrates the absorption spectra of

dye desorbing from the TiO₂ photoanode. Characteristic changes and blue shifts are observed in absorption pattern for TiO₂ loaded with dye. This blue shift is attributed to better deprotonation and less aggregation of the dye on TiO₂ surface [3, 9, 44, 45]. Increase in absorption intensity is observed for corresponding exposure to UV-O₃ treatment (0 min < 10 min < 30 min). This increase in absorption intensity of the photoanode sample exposed to UV-O₃ indicates efficient adsorption of the dye molecules on the TiO₂ surface due to removal of organic contamination there by providing better surface contact. This increase in dye loading capacity due to UV-O₃ exposure, leads to significant improvement in the current density of the fabricated DSSCs.

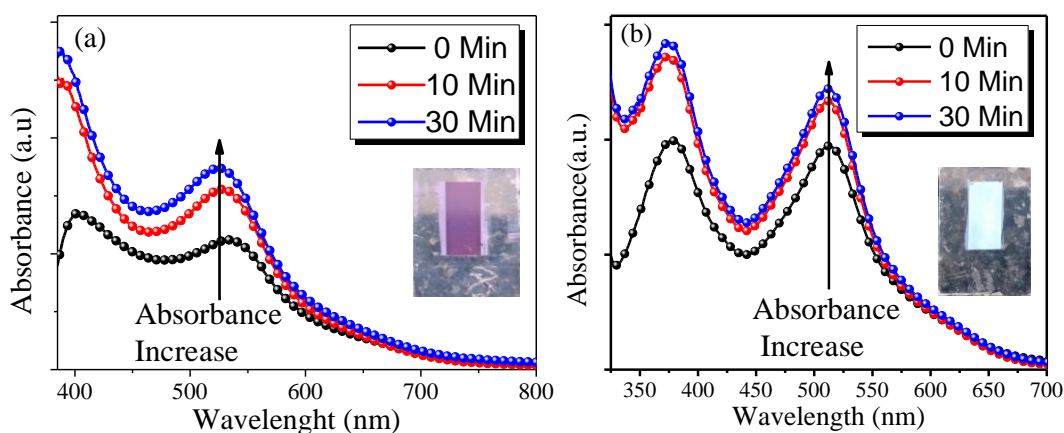


Fig. 5: UV-Visible absorption spectra of N719 dye (a) loaded on TiO₂ film, inset shows sensitized film and (b) dye solution desorbed from TiO₂ film, inset shows desorbed film.

Fig. 6 shows the Nyquist plots of electrochemical impedance spectra (EIS) for DSSCs along with the equivalent circuit (inset of fig. 6). EIS measurement of DSSCs is a powerful technique to study the charge transfer resistance and recombination reactions taking place at different interfaces in the solar cell i.e., first semicircle in the high-frequency region (from 1-100 kHz) explains the charge transfer resistance of counter electrode/electrolyte interface, second semicircle in the mid-frequency region (from 0.1 Hz-1 kHz) corresponds to the charge transfer resistance at photoanode/electrolyte interface, and in the low frequency region (from 0.1 Hz-0.01 Hz) provides information about diffusion resistance of the electrolytes [44, 46, 47]. The parameters of equivalent circuit as obtained by fitting the data are presented in Table S4. In the high frequency region, the onset point on the real axis of first semicircle corresponds to ohmic series resistance (R_s) of the

FTO substrate and TiO₂ catalytic film. The value of R_s decreases from 29.98Ω (0 min) to 20.25Ω (30 min) after UV-O₃ exposure. This decrease in R_s indicates better interfacial contact of the catalytic film on FTO leading to increase conductivity.

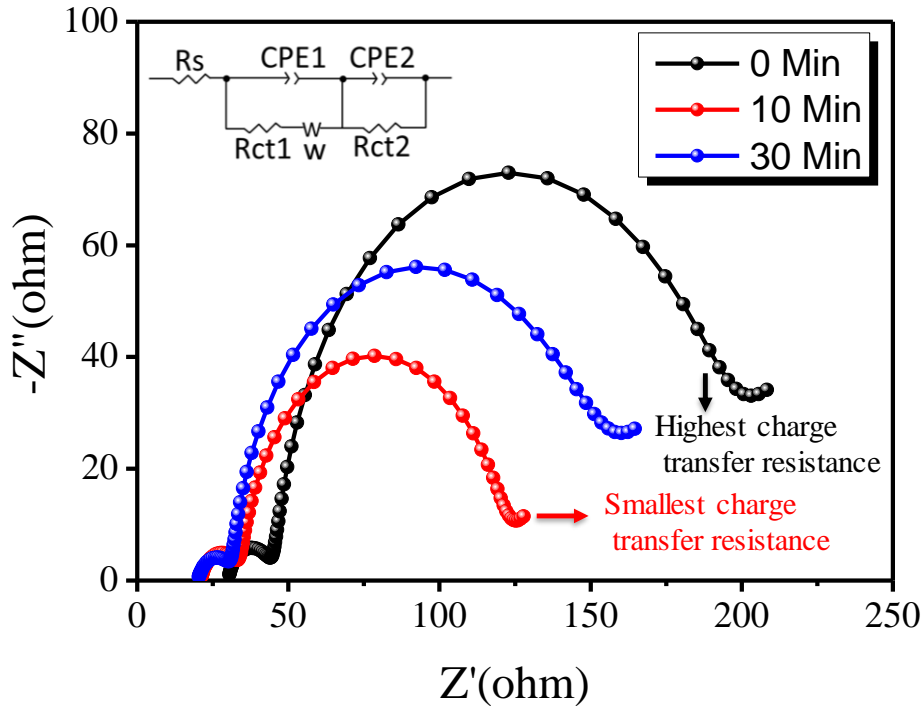


Fig. 6: Nyquist plot of DSSCs under the dark condition for different UV-O₃ treatment time.

The smallest semicircle (red colour) in the mid-frequency region for optimum 10 min treatment indicates substantial decrease in the charge transfer resistance, indicating minimum trap state, lower recombination rate, high electro-catalytic activity and faster diffusion of the electrolyte. Large semi-circle (black colour) for untreated device shows considerable charge transfer resistance leading to slower electronic transport, and increase in recombination reaction at the interface. This, results in overall lower performance of the DSSCs.

The electrical conductivity of TiO₂ ETL significantly influences the performance of DSSCs. With different UV-O₃ irradiation time, the linear scan of dark current (I) vs. voltage (V) curves of TiO₂ samples are shown in Fig. 7a. The slope of the I-V curves provides the electrical conductivity of the TiO₂ photoanode. This significant increase in I-V slope with increasing UV-O₃ exposure time is observed due to improved interfacial contact. UV-O₃ exposure of TiO₂ films may lead to enhanced conductivity due to the generation of oxygen vacancies [48, 49].

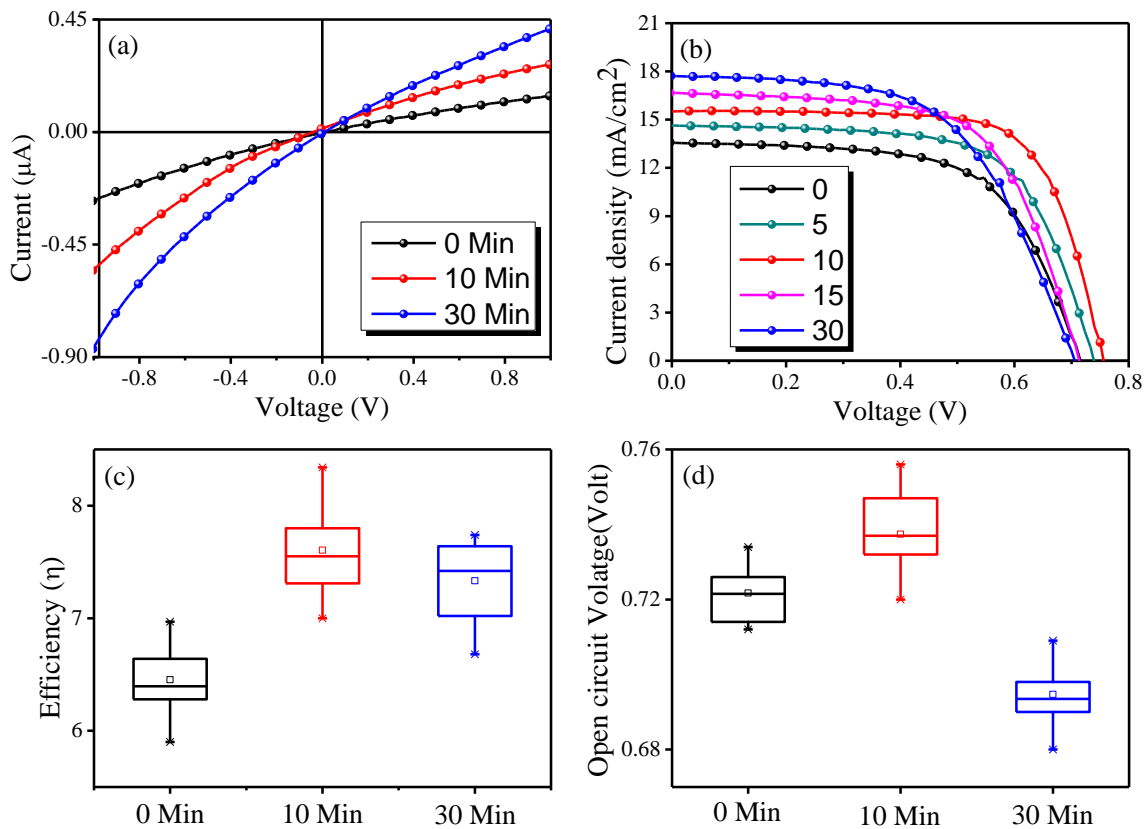


Fig. 7: Effect of UV-O₃ treatment on TiO₂ ETL (a) Dark linear *I-V* characteristics (b) Light *J-V* curve of DSSCs (c and d) Box chart of efficiency and open circuit voltage.

In order to understand the influence of UV-O₃ exposure, the performance of DSSCs *J-V* curve is displayed in Fig 7b. The PCE of DSSCs with different UV-O₃ exposure time are shown in Table S5. At 0 min, the photoelectric conversion efficiency (η) of DSSCs is 6.27% (V_{oc} =718.40 mV, J_{sc} = 13.02 mA/cm² and FF = 64.20%). The presence of residual organic contaminants on the TiO₂ film acts as recombination centre at the interface of TiO₂/ N719 dye/electrolytes thereby critically influencing the collection and transport of electrons, thus, affecting the overall efficiency of the DSSCs [33].

Compared to unexposed TiO₂ ETL, UV-O₃ exposure shows remarkable improvement in photoelectric conversion efficiency (Fig. 6c). By optimizing the duration of exposure, the best PCE of 8.34% achieved for 10 min with an increase of 33.01% efficiency (η = 6.27 to 8.34%), 16.27% photocurrent density (J_{sc} = 13.02 to 15.15 mA/cm²), 5.20% open circuit voltage (V_{oc} = 718.40 to 756 mV) and 10.74% fill factor (FF= 64.20 to 71.10%). The enhancement of PCE with UV-O₃

exposure may be attributed to fast electron transfer, increase in dye absorption, minimization of surface roughness and removal of organic binders [33-34]. However, the longer duration of UV-O₃ exposure time for 30 min gives no further enhancement in the performance of DSSCs. The efficiency decreases by 14.14% ($\eta = 8.34$ to 7.16%). This decrease in efficiency is attributed to lower V_{oc} , (Fig. 6d) and FF (Fig. S2) in overexposed surface may be due to the role of oxygen vacancies in facilitating carrier recombination at the TiO₂/dye interface [33-35, 48].

4 CONCLUSIONS

Herein, the effect of UV-O₃ exposure on the efficiency of the DSSCs has been carefully analysed and optimized. The fabricated device with optimized time for 10 min UV-O₃ exposure shows the best PCE of 8.34% ($J_{sc}=15.15$ mA/cm², $V_{oc}=756.00$ mV, FF=71.10%) with good reproducibility. However, any further increase in exposure time leads to decrease in the photo conversion efficiency of the solar cells. XRD and impedance curve measurement denotes enhanced crystallinity and decrease in the ohmic resistance of the electron transport layer. Thus higher efficiency for the optimally exposed solar cells may be due to removal of the organic contaminants as indicated by the increase in the oxygen vacancies (XPS results) or due to lowering of surface roughness as confirmed by the AFM results, leading to improved wettability and increase in the adsorption of dye to the TiO₂ surface. However, further research is required to clearly identify the inherent mechanism. Moreover, additional experiments can be performed to explore the effect of UV-O₃ exposure on the photocatalytic activity, electrical conductivity and the recombination reaction at the dye – TiO₂ interface; leading to better optimized parameters for the development of efficient solar cells.

ACKNOWLEDGEMENTS

This work was supported by the Department of Science and Technology, New Delhi, India through the projects DST/TSG/PT/2009/23 and IGSTC/MPG/PG(PKI)/2011A/48. G Lab Innovations (P) Ltd. Centre for Energy, Department of Chemistry, Department of Physics, and Central Instruments Facility IIT Guwahati are acknowledged for providing various instrument facilities.

Notes: The authors declare no competing financial interest.

References

- [1] B. Oregan, M. Grätzel, A Low-Cost, High-Efficiency Solar-Cell Based on Dye-Sensitized Colloidal TiO₂ Films, *Nature*, 353 (1991) 737-740.
- [2] S. Mathew, A. Yella, P. Gao, R. Humphry-Baker, B.F.E. Curchod, N. Ashari-Astani, I. Tavernelli, U. Rothlisberger, M.K. Nazeeruddin, M. Grätzel, Dye-sensitized solar cells with 13% efficiency achieved through the molecular engineering of porphyrin sensitizers, *Nat. Chem.*, 6 (2014) 242-247.
- [3] S. Zhang, H. Niu, Y. Lan, C. Cheng, J. Xu, X. Wang, Synthesis of TiO₂ Nanoparticles on Plasma-Treated Carbon Nanotubes and Its Application in Photoanodes of Dye-Sensitized Solar Cells, *J. Phys. Chem. C*, 115 (2011) 22025-22034.
- [4] A. Hadi, Q. Chen, M. Curioni, R. Xiao, T. Huang, Z. Liu, One-Step Fiber Laser Fabrication of Mesoporous and Compact TiO₂ Layers for Enhanced Performance of Dye-Sensitized Solar Cells, *ACS Sustainable Chem. Eng.*, 6 (2018) 12299-12308.
- [5] G.K. Mor, K. Shankar, M. Paulose, O.K. Varghese, C.A. Grimes, Use of Highly-Ordered TiO₂ Nanotube Arrays in Dye-Sensitized Solar Cells, *Nano Lett.*, 6 (2006) 215-218.
- [6] Y. Castro, N. Arconada, A. Durán, Synthesis and photocatalytic characterisation of mesoporous TiO₂ films doped with Ca, W and N, *Boletín de la Sociedad Española de Cerámica y Vidrio*, 54 (2015) 11-20.
- [7] T.B. Raju, J.V. Vaghasiya, M.A. Afroz, S.S. Soni, P.K. Iyer, Twisted donor substituted simple thiophene dyes retard the dye aggregation and charge recombination in dye-sensitized solar cells, *Org. Electron.*, 50 (2017) 25-32.
- [8] W.-Q. Wu, Y.-F. Xu, H.-S. Rao, C.-Y. Su, D.-B. Kuang, A double layered TiO₂ photoanode consisting of hierarchical flowers and nanoparticles for high-efficiency dye-sensitized solar cells, *Nanoscale*, 5 (2013) 4362-4369.
- [9] M. A. Afroz, K. K. Sonigara, T. B. Raju, S. S. Soni, P. K. Iyer, Effect of fluorine substitution and position on phenylene spacer in carbazole based organic sensitizers for dye sensitized solar cells, *Phys. Chem. Chem. Phys.*, 19 (2017) 28579-28587.
- [10] A. Hagfeldt, G. Boschloo, L. Sun, L. Kloo, H. Pettersson, Dye-Sensitized Solar Cells, *Chem. Rev.*, 110 (2010) 6595-6663.
- [11] M. Grätzel, Dye-sensitized solar cells, *J. Photochem. Photobiol. C*, 4 (2003) 145-153.

- [12] A. Sangiorgi, R. Bendoni, N. Sangiorgi, A. Sanson, B. Ballarin, Optimized TiO₂ blocking layer for dye-sensitized solar cells, *Ceram. Int.*, 40 (2014) 10727-10735.
- [13] M. S. Góes, E. Joanni, E. C. Muniz, R. Savu, T. R. Habeck, P. R. Bueno, F. Fabregat-Santiago, Impedance Spectroscopy Analysis of the Effect of TiO₂ Blocking Layers on the Efficiency of Dye Sensitized Solar Cells, *J. Phys. Chem. C*, 116 (2012) 12415-12421.
- [14] Tanvi, V. Saxena, A. Singh, O. Prakash, A. Mahajan, A. K. Debnath, K. P. Muthe, S.C. Gadkari, Improved performance of dye sensitized solar cell via fine tuning of ultra-thin compact TiO₂ layer, *Sol. Energy Mater. Sol. Cells*, 170 (2017) 127-136.
- [15] Z. A. Garmaroudi, M. Abdi-Jalebi, M. R. Mohammadi, R. H. Friend, A facile low temperature route to deposit a TiO₂ scattering layer for efficient dye-sensitized solar cells, *RSC Advances*, 6 (2016) 70895-70901.
- [16] J. Huo, Y. Tu, M. Zheng, J. Wu, Fabrication a thin nickel oxide layer on photoanodes for control of charge recombination in dye-sensitized solar cells, *J. Solid State Electrochem.*, 21 (2017) 1523-1531.
- [17] S. Thogiti, J.Y. Park, C.T. Thanh Thuy, D. K. Lee, B.-K. Min, H. J. Yun, J. H. Kim, High-Performance Dye-Sensitized Solar Cells through Graded Electron Transport in Band-Engineered W-TiO₂ Cascade Layer, *ACS Sustainable Chem. Eng.*, 6 (2018) 13025-13034.
- [18] J. Jun, M. Dhayal, J.-H. Shin, J.-C. Kim, N. Getoff, Surface properties and photoactivity of TiO₂ treated with electron beam, *Radiat. Phys. Chem.*, 75 (2006) 583-589.
- [19] P. M. Sommeling, B. C. O'Regan, R. R. Haswell, H. J. P. Smit, N. J. Bakker, J. J. T. Smits, J. M. Kroon, J. A. M. van Roosmalen, Influence of a TiCl₄ Post-Treatment on Nanocrystalline TiO₂ Films in Dye-Sensitized Solar Cells, *J. Phys. Chem. B*, 110 (2006) 19191-19197.
- [20] B. C. O'Regan, J. R. Durrant, P. M. Sommeling, N. J. Bakker, Influence of the TiCl₄ Treatment on Nanocrystalline TiO₂ Films in Dye-Sensitized Solar Cells. 2. Charge Density, Band Edge Shifts, and Quantification of Recombination Losses at Short Circuit, *J. Phys. Chem. C*, 111 (2007) 14001-14010.
- [21] H. Park, W.-R. Kim, H.-T. Jeong, J.-J. Lee, H.-G. Kim, W.-Y. Choi, Fabrication of dye-sensitized solar cells by transplanting highly ordered TiO₂ nanotube arrays, *Sol. Energy Mater. Sol. Cells*, 95 (2011) 184-189.

- [22] Q. Yi, S. Cong, H. Wang, Y. Wang, X. Dai, J. Zhao, Y. Sun, Y. Lou, G. Zou, High-stability Ti^{4+} precursor for the TiO_2 compact layer of dye-sensitized solar cells, *Appl. Surf. Sci.*, 356 (2015) 587-592.
- [23] K. Qi, S.-y. Liu, Y. Chen, B. Xia, G.-D. Li, A simple post-treatment with urea solution to enhance the photoelectric conversion efficiency for TiO_2 dye-sensitized solar cells, *Sol. Energy Mater. Sol. Cells*, 183 (2018) 193-199.
- [24] M. K. Parvez, G. M. Yoo, J. H. Kim, M. J. Ko, S. R. Kim, Comparative study of plasma and ion-beam treatment to reduce the oxygen vacancies in TiO_2 and recombination reactions in dye-sensitized solar cells, *Chem. Phys. Lett.*, 495 (2010) 69-72.
- [25] J. Tak Kim, S. Ho Kim, Surface modification of TiO_2 electrode by various over-layer coatings and O_2 plasma treatment for dye sensitized solar cells, *Sol. Energy Mater. Sol. Cells*, 95 (2011) 336-339.
- [26] J. Wang, Z. Lin, Dye-Sensitized TiO_2 Nanotube Solar Cells with Markedly Enhanced Performance via Rational Surface Engineering, *Chem. Mater.*, 22 (2010) 579-584.
- [27] F. D. Egitto, L. J. Matienzo, Transformation of Poly(dimethylsiloxane) into thin surface films of SiO_x by UV/Ozone treatment. Part I: Factors affecting modification, *J. Mater. Sci.*, 41 (2006) 6362-6373.
- [28] J. R. Vig, UV/ozone cleaning of surfaces, *J. Vac. Sci. Technol.*, A 3 (1985) 1027-1034.
- [29] L. Huang, X. Sun, C. Li, J. Xu, R. Xu, Y. Du, J. Ni, H. Cai, J. Li, Z. Hu, J. Zhang, UV-Sintered Low-Temperature Solution-Processed SnO_2 as Robust Electron Transport Layer for Efficient Planar Heterojunction Perovskite Solar Cells, *ACS Appl. Mater. Interfaces*, 9 (2017) 21909-21920.
- [30] B.-K. Lee, J.-J. Kim, Enhanced efficiency of dye-sensitized solar cells by UV- O_3 treatment of TiO_2 layer, *Curr. Appl. Phys.*, 9 (2009) 404-408.
- [31] K.-H. Park, M. Dhayal, High efficiency solar cell based on dye sensitized plasma treated nano-structured TiO_2 films, *Electrochem. Commun.*, 11 (2009) 75-79.
- [32] H. Liu, W. Yang, Y. Ma, Y. Cao, J. Yao, J. Zhang, T. Hu, Synthesis and Characterization of Titania Prepared by Using a Photoassisted Sol-Gel Method, *Langmuir*, 19 (2003) 3001-3005.
- [33] Y. Chu, H. Cai, L. Huang, Z. Xing, Y. Du, J. Ni, J. Li, J. Zhang, High-Efficient Flexible Perovskite Solar Cells with Low Temperature TiO_2 Layer via UV/Ozone Photo-Annealing Treatment, *Phys. Status Solidi A*, 216 (2019) 1800669.

- [34] Z. Wang, J. Fang, Y. Mi, X. Zhu, H. Ren, X. Liu, Y. Yan, Enhanced performance of perovskite solar cells by ultraviolet-ozone treatment of mesoporous TiO₂, *Appl. Surf. Sci.*, 436 (2018) 596-602.
- [35] X. Zhang, H. Tian, X. Wang, G. Xue, Z. Tian, J. Zhang, S. Yuan, T. Yu, Z. Zou, The role of oxygen vacancy-Ti³⁺ states on TiO₂ nanotubes' surface in dye-sensitized solar cells, *Mater. Lett.*, 100 (2013) 51-53.
- [36] H. Liu, W. Yang, Y. Ma, J. Yao, Extended visible light response of binary TiO₂-Ti₂O₃ photocatalyst prepared by a photo-assisted sol-gel method, *Applied Catalysis A*, 299 (2006) 218-223.
- [37] R. Liu, W.-D. Yang, L.-S. Qiang, Enhanced efficiency for dye-sensitized solar cells using a surface-treated photo-anode, *J. Power Sources*, 199 (2012) 418-425.
- [38] A. Rudawska, E. Jacniacka, Analysis for determining surface free energy uncertainty by the Owen-Wendt method, *Int. J. Adhes. Adhes.*, 29 (2009) 451-457.
- [39] J. Wu, H. Lin, P. Kuo, B. Su, S. Chu, Y. Chen, S. Liu, C. Chang, C. Wu, Effect of UV-Ozone Treatment on the Performance of ZnO TFTs Fabricated by RF Sputtering Deposition Technique, *IEEE Trans. Electron Devices*, 61 (2014) 1403-1409.
- [40] R. Wang, K. Hashimoto, A. Fujishima, M. Chikuni, E. Kojima, A. Kitamura, M. Shimohigoshi, T. Watanabe, Photogeneration of Highly Amphiphilic TiO₂ Surfaces, *Adv. Mater.*, 10 (1998) 135-138.
- [41] N. Sakai, R. Wang, A. Fujishima, T. Watanabe, K. Hashimoto, Effect of Ultrasonic Treatment on Highly Hydrophilic TiO₂ Surfaces, *Langmuir*, 14 (1998) 5918-5920.
- [42] B.-G. Kim, J.-Y. Kim, S.-J. Lee, J.-H. Park, D.-G. Lim, M.-G. Park, Structural, electrical and optical properties of Ga-doped ZnO films on PET substrate, *Appl. Surf. Sci.*, 257 (2010) 1063-1067.
- [43] S. Saekow, W. Maiakgree, W. Jarernboon, S. Pimanpang, V. Amornkitbamrung, High intensity UV radiation ozone treatment of nanocrystalline TiO₂ layers for high efficiency of dye-sensitized solar cells, *J. Non-Cryst. Solids*, 358 (2012) 2496-2500.
- [44] E. Dell'Orto, L. Raimondo, A. Sassella, A. Abbotto, Dye-sensitized solar cells: spectroscopic evaluation of dye loading on TiO₂, *J. Mater. Chem.*, 22 (2012) 11364-11369.

- [45] D. Chandra, T. Ohji, K. Kato, T. Kimura, Ligand-Assisted Fabrication of Small Mesopores in Semi-Crystalline Titanium Oxide Films for High Loading of Ru(II) Dyes, *Langmuir*, 27 (2011) 11436-11443.
- [46] M.S. Ansari, R. Maragani, A. Banik, R. Misra, M. Qureshi, Enhanced photovoltaic performance using biomass derived nano 3D ZnO hierarchical superstructures and a D–A type CS-Symmetric triphenylamine linked bithiazole, *Electrochim. Acta*, 259 (2018) 262-275.
- [47] F. Fabregat-Santiago, G. Garcia-Belmonte, I. Mora-Seró, J. Bisquert, Characterization of nanostructured hybrid and organic solar cells by impedance spectroscopy, *Phys. Chem. Chem. Phys.*, 13 (2011) 9083-9118.
- [48] T. Wang, D. Ding, H. Zheng, X. Wang, J. Wang, H. Liu, W. Shen, Efficient Inverted Planar Perovskite Solar Cells Using Ultraviolet/Ozone-Treated NiOx as the Hole Transport Layer, *Sol. RRL.*, 3 (2019) 1900045.
- [49] R. Islam, G. Chen, P. Ramesh, J. Suh, N. Fuchigami, D. Lee, K. A. Littau, K. Weiner, R.T. Collins, K. C. Saraswat, Investigation of the Changes in Electronic Properties of Nickel Oxide (NiOx) Due to UV/Ozone Treatment, *ACS Appl. Mater. Interfaces*, 9 (2017) 17201-17207.